

# Broken symmetry states and Quantum Hall Ferromagnetism in decoupled twisted bilayer graphene

Vineet Pandey,<sup>†</sup> Prasenjit Ghosh,<sup>†</sup> Riju Pal,<sup>‡</sup> Sourav Paul,<sup>†</sup> Abhijith M B,<sup>†</sup> Kenji  
Watanabe,<sup>¶</sup> Takashi Taniguchi,<sup>§</sup> Atindra Nath Pal,<sup>‡</sup> and Vidya Kochat<sup>\*,†</sup>

<sup>†</sup>*Materials Science Centre, Indian Institute of Technology, Kharagpur, West Bengal -  
721302, India*

<sup>‡</sup>*S. N. Bose National Centre for Basic Sciences, Kolkata, West Bengal -700106, India*

<sup>¶</sup>*Research Center for Electronic and Optical Materials, National Institute for Materials Science,  
1-1 Namiki, Tsukuba 305-0044, Japan*

<sup>§</sup>*Research Center for Materials Nanoarchitectonics, National Institute for Materials Science, 1-1  
Namiki, Tsukuba 305-0044, Japan*

E-mail: vidya@matsc.iitkgp.ac.in

## Abstract

Twisted bilayer graphene (TBLG) with large twist angle is a novel 2D bilayer system with strong interlayer Coulomb interactions, whilst suppressed interlayer carrier tunneling due to momentum mismatch between the Dirac cones of individual graphene layers. This interlayer decoherence disentangles the layer degree of freedom from spin-valley space. We demonstrate the role of charge screening effects in electronically decoupled TBLG that determines the Landau level (LL) crossings and multicomponent Quantum Hall (QH) effect resulting from combinations of broken symmetry states with spin and valley flavors of constituent layers.

The  $N = 0$  LL at zero filling factor is characterized by a field-induced Kosterlitz-Thouless transition to an ordered ground state, consistent with predictions of intervalley coherent state of Kekulé order. Pronounced hysteresis and electron-hole asymmetry observed in the QH regime suggests pinning of low-energy topological excitations, i.e., skyrmions with spin and valley textures, at charged defects in graphene channel.

**Keywords:** twisted bilayer graphene, broken symmetry states, Quantum Hall Ferromagnetism, skyrmions.

Multicomponent Quantum Hall (QH) effect<sup>1</sup> offer rich physics and interesting phenomena manifested from the various degeneracies underlying the Hamiltonian of the material system. This arises from additional degrees of freedom such as the electron spin, valley index in multi-valley materials and also the layer index in 2D electron gas systems (2DEGS) with multiple quantum well structures or 2D bilayers.<sup>2-4</sup> The multicomponent Hamiltonian of such material systems in the presence of magnetic field have revealed novel fractional QH states, spontaneously broken symmetries, QH ferromagnetic phases and phase transitions.<sup>5-11</sup> 2DEGS of modulation-doped semiconductor heterostructures were a test bed to understand the role of Coulomb interactions in Landau levels (LL) with multiple degenerate degrees of freedom. The spatial ordering of pseudospin/isospin degrees of freedom such spin, layer number, LL index led to a new class of condensed matter systems termed as QH Ferromagnets. Similar QH ferromagnetic phases characterized by interaction-induced gaps and broken symmetries at integer filling factors have been observed in various graphene systems such as single/bi/tri/rhombohedral stacked multilayer graphene attributed to the spin-valley degeneracy in graphene.<sup>12-21</sup> The low energy band structure of monolayer graphene is described by two flavours of massless Dirac fermions at the inequivalent K and K' valleys of the hexagonal Brillouin zone. This valley degeneracy combines with spin degeneracy giving rise to the anomalous QH sequence of  $\sigma_{xy} = \pm \frac{4e^2}{h} \left( N + \frac{1}{2} \right)$  at high magnetic fields.<sup>22,23</sup> In a graphene LL, this four fold spin-valley degeneracy is described by a single  $SU(4)$  isospin and gives rise to ferromagnetic instabilities driven by exchange interactions with order parameter corresponding to a finite polarization in spin and/or valley space. This results in finite charge excitation gaps at integer filling factors within the quartet LL manifested as QH isospin ferromagnetic states.<sup>12,24,25</sup>

The QH phenomena in semiconductor heterostructure-based bilayer 2DEG revealed additional broken symmetries arising from competing energies including cyclotron energy, Zeeman spin-splitting, intra- and interlayer Coulomb interactions along with interlayer tunnel coupling which leads to LL mixing.<sup>26-31</sup> TBLG can be considered as a unique bilayer 2DEG with two mutually rotated single layers with interlayer Coulomb interactions and tunnelling in the extremity of a sub-

nm tunnel barrier of 0.4 nm. At twist angles of  $1.05^\circ$ , called the magic angles, Dirac cones from each layer hybridize to form flat bands, thereby leading to strong coupling of the layers.<sup>32–34</sup> At larger twist angles, the Dirac cones of each layer are significantly displaced in the momentum space and this resultant momentum mismatch strongly suppresses interlayer coherence. As opposed to Bernal-stacked bilayer graphene in which the layer and valley degrees of freedom are correlated, the larger twist angles in TBLG unties the layer degree of freedom from the spin and valley degeneracies in individual layers, which gives rise to eight-fold degenerate LLs.<sup>35,36</sup> Thus TBLG at intermediate and large twist angles presents an exciting platform to study multicomponent QHE and effects of strong intra- and inter-layer Coulomb interactions. In this work, we report the observation of broken symmetry QH states in the zeroth and higher order LL octets of high mobility TBLG in the decoupled regime. The observed LL filling factors are understood in terms of charge screening effects leading to different filling rates for the LLs of individual layers. We present strong evidence of magnetic field-induced Kosterlitz-Thouless transition at zero filling factor in decoupled TBLG and the emergence of QH ferromagnetic states dominated by pinned skyrmion lattices with spin and valley flavours.

TBLG devices in h-BN encapsulated Hall bar geometry were fabricated using the van der Waals pick-up and edge contact technique.<sup>37</sup> Randomly stacked h-BN/TBLG/h-BN heterostructures were characterized using Raman spectroscopy<sup>38,39</sup> and the twist angles were estimated to be  $\sim 5^\circ$  and  $18^\circ$  for devices D1 and D2 respectively (See Supporting Information, section S1). The higher twist angles were specifically chosen to ensure that the interlayer coherent transport is minimal and also the accessible Fermi level modulation is much below the saddle point energies due to hybridization of the Dirac cones from individual layers. Fig. 1a depicts the measurement configuration for the devices D1 and D2 from which the longitudinal resistance,  $R_{xx}$  is plotted as a function of total carrier density ( $n_{\text{tot}}$ ) at temperature of 1.6 K and 300 K as shown in Fig. 1b. The extremely high mobility in D1 (estimated to be  $\sim 200,000 \text{ cm}^2\text{V}^{-1}\text{s}^{-1}$  at 1.6 K) enabled observation of QHE commencing at very low fields of 1 T, with  $R_{xx}$  values going to zero and appearance of additional  $R_{xx}$  minima above 3T as can be seen in the Landau fan diagram in Fig. 1c. In Fig. 1d, we plot

the  $R_{xx}$  and the Hall resistance  $R_{xy}$  at 1.6 K and 9 T as a function of the total filling factor,  $\nu_{tot} = n_{tot}h/eB$ , where  $n_{tot}$  is the total charge carrier density from the two graphene layers and  $B$  is the applied magnetic field. If the TBLG is considered a system of two independent monolayers, then  $R_{xx}$  minima are expected at integer filling factors of  $\nu_{tot} = 2\nu_{SLG} = \pm 4, \pm 12, \pm 20, \pm 28, \dots$ . On the contrary,  $R_{xx}$  minima occurs for  $\nu_{tot} = \pm 4, \pm 8, \pm 12, \pm 16, \dots$  similar to Bernal-stacked BLG indicating an eight-fold degenerate zero LL.<sup>35,36</sup>

Our experiments focussed on single-gated TBLG physics which results in different charge carrier densities in the upper and lower graphene layers as the back-gate field is varied. This is a consequence of the low density of states in graphene leading to incomplete screening of the gate field by the lower layer. This charge carrier imbalance between the two layers results in a beating pattern in the Shubnikov-de Haas (SdH) oscillations measured in the  $R_{xx}$  of D1 as illustrated in Fig. 2a. In order to determine the charge carrier density of individual layers, the Fast Fourier Transform (FFT) of  $\Delta R_{xx}$  ( $R_{xx}$  oscillations centered around zero) vs.  $1/B$  was performed for different  $n_{tot}$  as shown in Fig. 2b. This yielded two prominent peaks corresponding to the two frequencies ( $f_{U,L}$  for upper and lower layers) involved in the SdH oscillations, which can be translated to carrier densities of upper and lower layers defined as  $n_U$  and  $n_L$  through the relation  $n_{U,L} = g e f_{U,L} / h$ , where  $g$  is the degeneracy factor of 4 arising from four-fold spin-valley degeneracy in each graphene layer. We attribute the larger frequency to the carrier density of lower layer due to the stronger influence of the gate field. The carrier densities of the individual layers estimated from SdH oscillations along with  $n_{tot}$ , where  $n_{tot} = n_U + n_L$  is plotted in Fig. 2c. These carrier density values agree well with the theoretical estimates from a model employed for calculation of carrier densities of independently contacted graphene double layers separated by a thin dielectric.<sup>40,41</sup> The dashed straight lines show the fitting using this model from which we extract the interlayer capacitance of the TBLG system as  $5.7 \pm 1 \mu\text{F cm}^{-2}$  which agrees well with previously reported values (See Supporting Information, section S2).<sup>41,42</sup>

Though the overall QH sequence resembles Bernal-stacked BLG, several QH states present distinct evolution with increasing magnetic field as evident from the Figs. 2d,e in which the Hall con-

ductivity,  $\sigma_{xy}$  is plotted as a function of  $n_{tot}$  for hole and electron regimes. Certain QH plateaus vanish at large  $B$  as observed for  $\pm v_{tot} = 20, 40$ , while some other QH plateaus emerge at high  $B$  such as  $\pm v_{tot} = 36$ . In addition, we observe disappearance of QH plateau  $\pm v_{tot} = 28$  at  $B \sim 1.5$  T which then re-emerges at fields higher than 3.5 T. These correspond to LL crossings marked by a change in the QH sequence and can be attributed to the charge carrier imbalance between the individual layers in TBLG.<sup>43</sup> The schematic in Fig. 2f represents the filling of the LL of lower and upper layers where the increased gap between the LLs in the upper layer depicts additional charging energy required to fill these LLs as compared to the lower layer. The filling of the first LL of the lower layer renders this layer incompressible, compelling the next induced charges to fill the upper layer LL. The subsequent LL of the lower layer turns compressible before or after the upper layer LL is completely filled depending on the charging energy for filling the upper layer LL and the LL gap in the lower layer. Such layer dependent LL filling in TBLG is especially important at larger filling factors due to the strong displacement field between the graphene layers induced by large gate voltage which is evident from calculations of  $n_L$  and  $n_U$  using the above explained model where the linear energy dispersion is replaced with LL energies in graphene (see Supporting Information, section S2). This picture explains the presence of QH states at  $\pm v_{tot} = 8, 16, 24, 32, \dots$  due to filling of individual graphene layer LL corresponding to  $[v_U, v_L] = [2, 6], [6, 10], [10, 14], [14, 18], \dots$  corresponding to the filling of LL of SLG at  $\pm v = 2, 6, 10, 14, 18, \dots$ . The LL crossings observed as a function of magnetic field at high  $V_g$  in Fig. 2g can also be understood in terms of  $v_{tot}$  transforming between two different combinations of  $v_U$  and  $v_L$ , for instance,  $v_{tot} = 20$  transforming from  $[10, 10]$  to  $[6, 14]$  or  $v_{tot} = 28$  from  $[14, 14]$  to  $[10, 18]$ .

The evolution of QHE with increasing magnetic fields in device D1 displayed notable features as shown in Figs. 3a-b, such as highly insulating state at  $v_{tot} = 0$  and additional  $R_{xx}$  minima in the  $N = 0$  LL at  $v_{tot} = \pm 2$  and also at odd filling factors of  $v_{tot} = \pm 1, \pm 3$  above fields of 2 and 4 T respectively corresponding to broken symmetry phases. Such  $R_{xx}$  dips were observable in the  $N \geq 1$  LLs as well, but not as distinct as in  $N = 0$  LL. We attempt to understand the origin of these broken symmetry states as arising from  $SU(4)$  isospin space consisting of spin and valley

degrees of freedom in the individual layers of TBLG. The strong exchange interactions between the electrons in LLs of graphene lifts the spin-valley degeneracy giving rise to QH ferromagnets with polarized or coherent superposition of spin, valley and layer degrees of freedom.<sup>24</sup> In the half-filled LLs ( $\pm\nu = 0, 4, 8, \dots$ ) of graphene characterized by double occupancy of each cyclotron guiding centre, Pauli exclusion principle prevents simultaneous polarization in spin and valley space, whereas in the quarter-filled LLs ( $\pm\nu = 1, 3, 5, \dots$ ) the single occupancy of cyclotron guiding centers can lead to simultaneous spin and valley polarization.<sup>12</sup> Transport measurements in tilted  $B$  have resolved the spin-polarized character of the different QHS. For the  $N = 0$  LL, spin textured charged excitations are favoured for  $\nu = \pm 1$  in contrast to the  $N \neq 0$ , where Zeeman anisotropy dominates leading to spin polarized ground states at half-filling and charged excitations with valley flip textures at quarter filling.<sup>12</sup> Considering the scenario of unequal LL filling of upper and lower layers due to screening of the gate field,  $R_{xx}$  minima observed at all the integer filling factors of zero LL of D1 can be explained as arising from the broken symmetries of a combination of fully-filled, half-filled and quarter-filled LLs of both layers which is given in Table 1. The asymmetry observed in the electron and hole side can possibly arise due to residual disorder which can affect the broken symmetry states. In addition, the QH states showed striking variations with the gate sweep directions as can be seen from Fig. 3a,b. Contrary to Fig. 3a, we observed prominent dips on the hole regime compared to the electron regime in Fig. 3b when the gate voltage was swept from negative to positive values. While the  $R_{xx}$  minima in the electron regime remained at the same integer values, the additional minima in the  $N = -1, -2$  LLs vanished. The broken symmetry states are also observed in the magnetic field dependence of  $R_{xx}$  as additional minima, along with corresponding plateaus in  $R_{xy}$ , at different carrier densities which are marked in Fig. 3c,d.

In D1, the  $\nu_{tot} = 0$  insulator phase and the other broken symmetry phases displayed activated temperature dependence. The QH insulator gap at  $\nu_{tot} = 0$  is estimated for magnetic fields of 5 T and 9 T to be 0.71 meV and 1.75 meV respectively on fitting longitudinal resistivity with Arrhenius equation which is shown in Fig. 3e. This is a clear indication of increased energy gaps at higher  $B$  for  $\nu_{tot} = 0$  state. Out of the theoretically predicted possible QH ferromagnetic states

Table 1: Observed QH states and its contributing LLs (*Fully-filled (FF)*, *Half-filled (HF)*, and *Quarter-filled (QF)* states):

<b>Total filling factor, <math>\nu_{\text{tot}}</math></b>	<b>Landau Level, <math>N = 0</math> or <math>1</math>, <math>(N_U, N_L)</math></b>	<b>Combination of upper layer and lower layer, <math>[\nu_U, \nu_L]</math></b>
$\pm 1$	(0,0)	$[0, \pm 1]$ , {HF, QF}
$\pm 2$	(0,0)	$[\pm 1, \pm 1]$ , {QF, QF}
$\pm 3$	(0,0)	$[\pm 1, \pm 2]$ , {QF, FF}
$\pm 5$	(0, $\pm 1$ )	$[\pm 2, \pm 3]$ , {FF, QF}
$\pm 6$	(0, $\pm 1$ )	$[\pm 2, \pm 4]$ , {FF, HF}

at charge neutrality such as valley-polarized charge density wave phase, spin ferromagnet, canted antiferromagnet and valley-polarized Kekulé bond order, recent scanning tunneling spectroscopic (STS) studies provide direct evidence of a magnetic field-tuned transition to an intervalley coherent state (IVC) with a Kekulé reconstruction that is spin-unpolarized and characterized by a real-space electronic wave function whose probability density is spread on both the sublattices.<sup>44–48</sup> The huge increase in  $R_{xx}$  at  $\nu_{\text{tot}} = 0$  (defined as  $R_0$ ) is indicative of a high-field ordered state of a QH insulator.<sup>49,50</sup> We present evidence of this in Fig. 3f where  $R_0 \sim \xi(h^2)$ , where the correlation length  $\xi$  has Kosterlitz-Thouless (KT) dependence given by<sup>51</sup>

$$\xi_{KT} \sim \exp(b/\sqrt{1-h}) \quad (1)$$

with  $h = B/B_0$ . We plot  $\log R_0$  vs  $\sqrt{1-h}$  in Fig. 3f, in which the high- $B$  region is linear on putting  $B_0$  to  $\sim 11$  T which is extracted from the plot of  $(d \ln R_0 / dH)^{-2/3}$  vs  $B$  (See inset). From the slope,  $b \sim 0.75$ , which agrees with standard KT theory.<sup>51</sup> The KT behavior at the  $\nu = 0$  state in graphene agrees well with the theories that predict a valley pseudospin ordering giving rise to a XY pseudospin ferromagnet with  $U(1)$  symmetry, through a spontaneously generated hybridization of the electron wavefunctions associated with the  $K$  and  $K'$  valleys.<sup>49</sup> As the  $N = 0$  LLs associated with the  $K$  and  $K'$  valleys localize on  $B$  and  $A$  sublattices respectively, the lattice translational symmetry is also broken resulting in a bond density wave or Kekulé order. In the clean limit, the



ground state is an XY ordered phase formed from charge-neutral bound vortex-antivortex (V-AV) pairs, in which the Coulomb exchange favours fully valley polarized state where the z-component of the pseudospin of the pair points in the same direction. Charged impurities can induce and pin charged V-AV pairs whose binding interactions are screened either by increasing impurity density or reducing magnetic field.<sup>49</sup> This leads to unbinding of charged V-AV pairs triggering KT transition to a disordered phase at low  $B$  that contributes to electrical transport and reduction of resistance as we have observed in Fig. 3a,b.

A closer look at the gate sweeps of  $R_{xx}$  and  $R_{xy}$  reveal considerable hysteresis between the sweep directions, especially at the negative filling factors and between  $\nu_{tot} = -4$  to  $+4$  along with notable change in the resistance values as shown in Figs. 4a-d. We observe a peak in the  $R_{xy}$  in both sweeps directions at  $\nu_{tot} = 0$ , with opposite trends for the peak values  $R_{xx}$  and  $R_{xy}$ . The total resistivity at a particular  $B$  is the determinant of the resistivity tensor which remains constant though the relative magnitude of the contributions from longitudinal and transverse components may vary due to disorder configuration, which holds true for the resistance values changes with sweep direction for other filling factors as well. We first address the origin of hysteresis in the  $\nu_{tot} = 0$  QH insulator state. We have already established from the observed KT transition that the QH insulator state is attributed to Kekulé bond order. STS studies have shown direct observation of topological excitations of the IVC phase by visualizing valley skyrmions near charged defects, whose valley texture resembles canted antiferromagnetic skyrmion excitation of the Kekulé order.<sup>44,45,52</sup> In graphene LL at  $\nu = \pm 1$ , corresponding to quarter filling, where Zeeman anisotropy is not dominant, all the electrons (or holes) spontaneously align their spin to reduce the Coulomb interaction. Instead of spin-flip transitions, this spin-polarization happens through formations of skyrmions carrying a charge of  $\pm e$  due to their lower energy.<sup>12,25</sup> Such skyrmion spin textures have also been observed in earlier experiments in the half-filled LLs in graphene at  $\nu = \pm 4, \pm 8$  where exchange energy dominates Zeeman anisotropy in agreement with theoretical predictions that show that lowest energy charged excitations in graphene for  $N \leq 3$  are skyrmions.<sup>25,53</sup> For quarter-filled  $N = \pm 1, 2, 3$  LLs of graphene, valley textured skyrmions have been predicted and

seen in transport experiments.<sup>54</sup> In short, skyrmion lattice states possibly dominate the broken symmetry QH phases in the  $N \leq 2$  LLs of the individual graphene layers of our TBLG device D1. As the skyrmions carry a charge of  $\pm e$ , they can be pinned at by charged defects having the opposite charge of the skyrmion. The residual n-doping in our device can thus lead to pinning of the skyrmions on the hole side, which can result in the hysteresis observed upto large hole filling factors during the gate sweep, while the hysteresis almost vanishes for the electron filling factors in  $N \geq 1$  LLs as is evident in Figs. 4b,d. The hysteresis is absent at low  $B$  (3T) as can be seen in Fig. 4e (i). Temperature dependence of the QH ferromagnetic states shown in Fig. 4e (ii) and (iii) reveal the vanishing of hysteresis in  $R_{xx}$  and  $R_{xy}$  at temperatures  $\sim 15$  K. The observation of hysteresis only at high  $B$  and low temperature in the regime where QH ferromagnetism develops relates well with pinned skyrmion lattice picture.

In conclusion, we have studied the interplay of charge screening effects and Landau level crossings to understand the integer QHE in decoupled TBLG. A comprehensive understanding of the multicomponent Quantum Hall effect is provided on the basis of combinations of broken symmetry states from independent layers of the TBLG. The Kosterlitz-Thouless transition into an ordered ground state of Kekulé order at zero LL filling factor and hysteretic QH ferromagnetism due to pinned spin and/or valley skyrmions reveal that decoupled graphene bilayers can be intriguing systems to study quantum phases and phase transitions.

## FIGURES

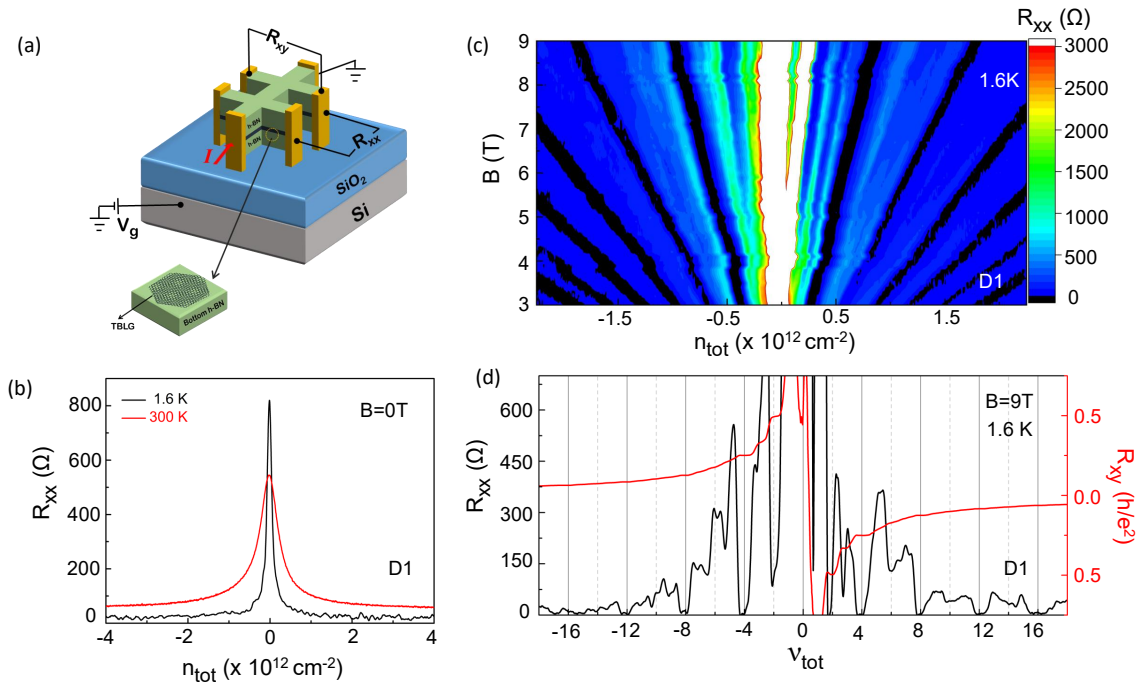


Figure 1: (a) Schematic illustration of the bottom-gated h-BN encapsulated TBLG in Hall bar geometry. (b)  $R_{xx}$  as a function of  $n_{\text{tot}}$  measured at  $1.6 \text{ K}$  and  $300 \text{ K}$  under  $B = 0 \text{ T}$  for device D1. (c) Landau fan diagram showing  $R_{xx}$  as a function of  $B$  and  $n_{\text{tot}}$  at  $1.6 \text{ K}$ . (d)  $R_{xx}$  and  $R_{xy}$  plotted as a function of  $v_{\text{tot}}$  at  $B = 9 \text{ T}$  and  $1.6 \text{ K}$ .

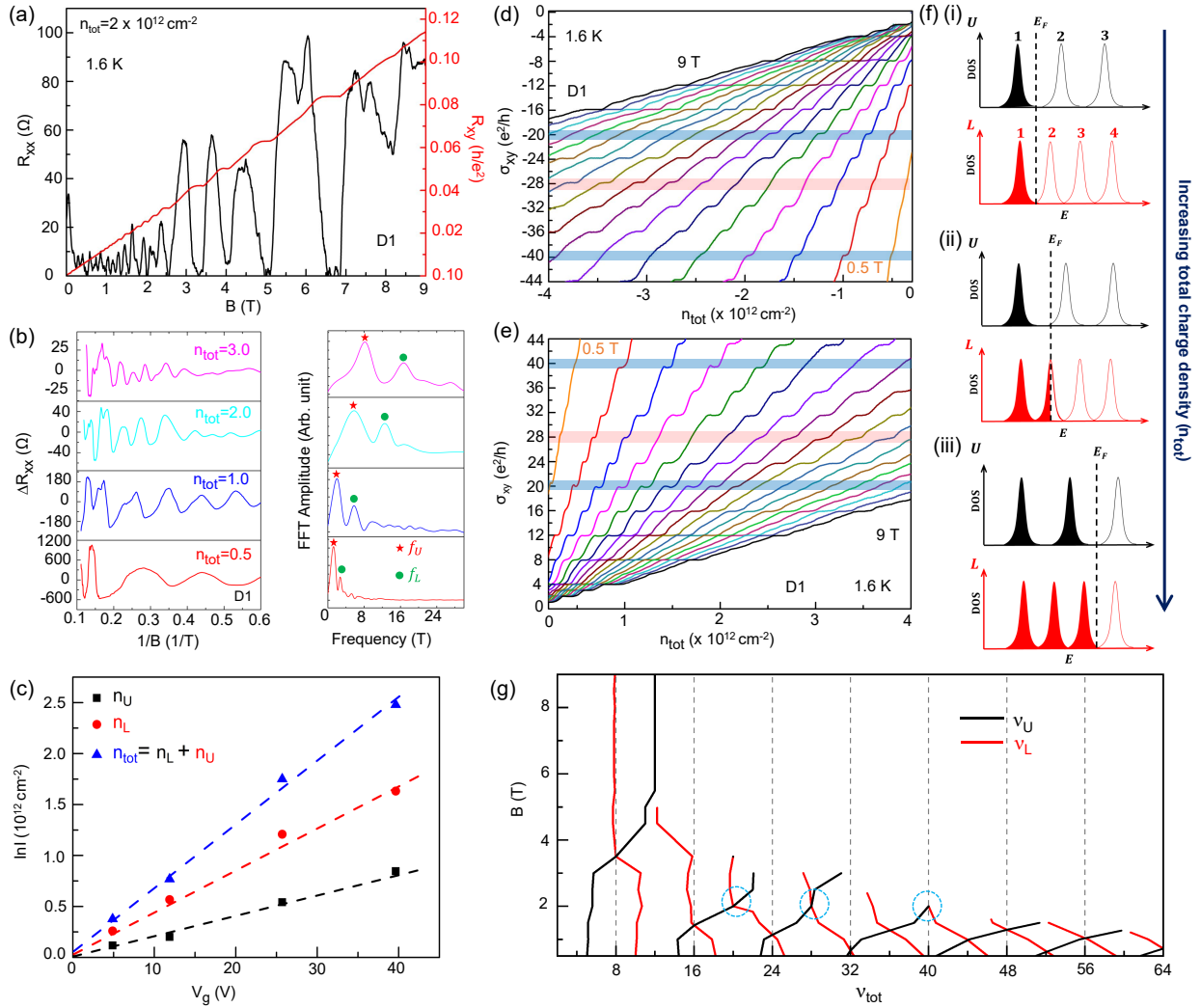


Figure 2: (a)  $R_{xx}$  and  $R_{xy}$  as a function of  $B$  at 1.6 K for a fixed  $n_{tot} \approx 2.0 \times 10^{12} \text{ cm}^{-2}$ . (b)(Left)  $\Delta R_{xx}$  vs.  $1/B$  for different  $n_{tot}$  ( $\times 10^{12} \text{ cm}^{-2}$ ) values at 1.6 K. (Right) Corresponding FFT for each  $n_{tot}$ , displaying two frequencies,  $f_U$  and  $f_L$  which represent the upper and lower layers, respectively. (c) Upper layer ( $n_U$ ), lower layer ( $n_L$ ), and total ( $n_{tot} = n_L + n_U$ ) carrier densities as function of gate voltage ( $V_g$ ). The symbols represent experimental data estimated from the FFT in (b), while the dashed lines denote theoretical values estimated from graphene double layer model. (d) and (e) Hall conductivity ( $\sigma_{xy}$ ) vs.  $n_{tot}$  at 1.6 K measured at different  $B$  values between 0.5 and 9 T in steps of 0.5 T for hole and electron doping regimes respectively. Blue strips indicate the disappearance, and red strips indicate the reappearance of QH states. (f) (i)–(iii) Schematic illustration of the filling of LLs of upper (U) and lower (L) graphene layers of TBLG due to partial screening of gate electric field by the lower graphene layer. (g) Calculated  $v_{tot}$  (see Supporting Information, section S2) as a function of  $B$ , along with  $v_U$  (black) and  $v_L$  (red) for device D1 at 1.6 K. The plot shows distinct LL crossings ( $v_{tot} = \pm 20, \pm 28, \pm 40$ , etc.) highlighted with blue circles.

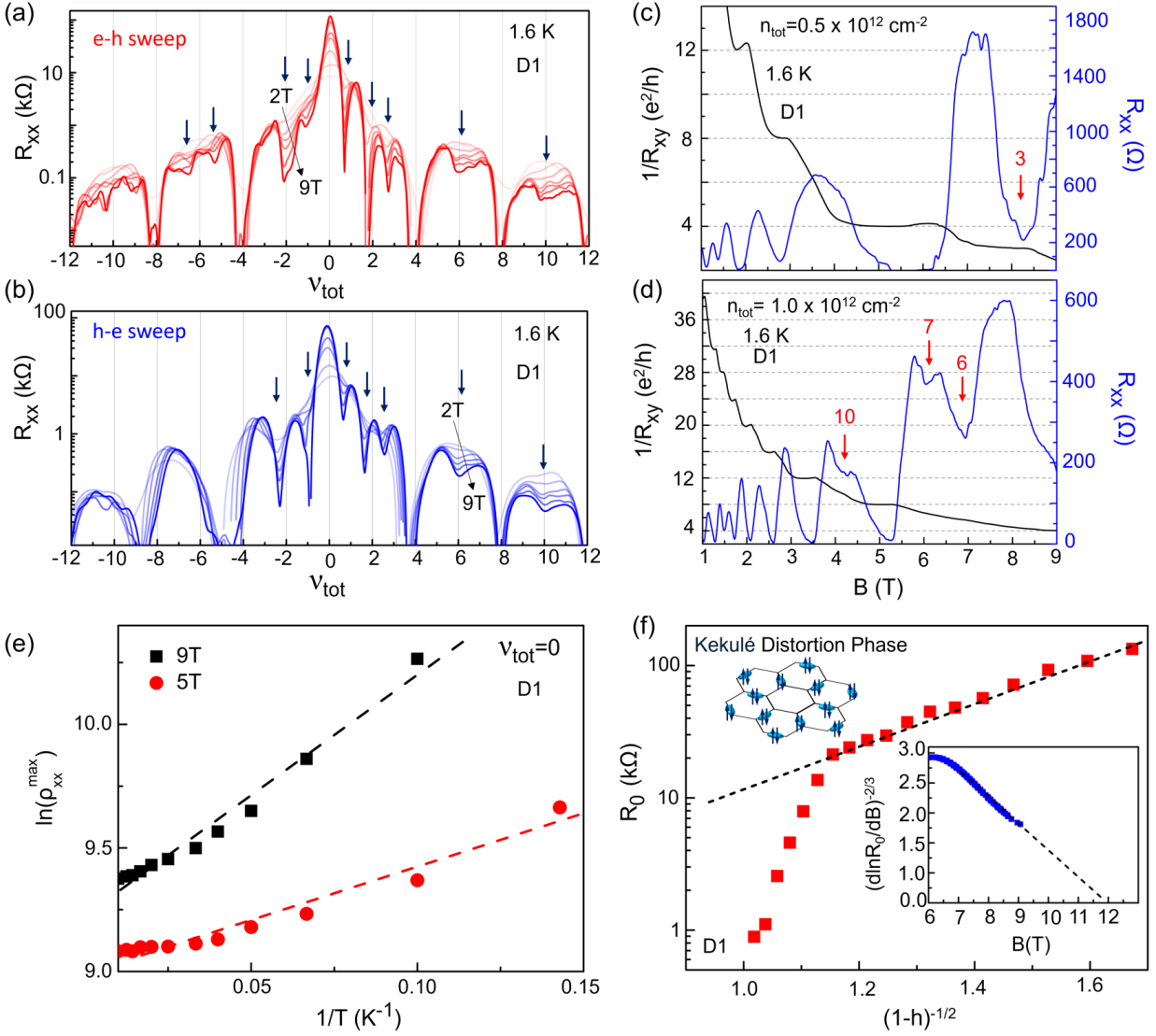


Figure 3: (a) and (b) show the logarithmic scale of  $R_{xx}$  as a function of  $v_{tot}$  at different  $B$  values ranging from 2 T to 9 T at 1.6 K for positive to negative (e-h) and negative to positive (h-e) voltage sweeps, respectively. Various broken symmetry QH states (see Table T-1) are indicated with arrows. (c) and (d) show  $1/R_{xy}$  and  $R_{xx}$  as function of  $B$  at  $n_{tot} = 0.5$  and  $1.0 (\times 10^{12} \text{ cm}^{-2})$ , respectively, at 1.6 K. Various broken symmetry states are indicated by  $R_{xx}$  dips and QH plateaus are marked with red arrows. (e) Plot of  $v = 0$  resistivity,  $\ln(\rho_{xx}^{max})$  vs.  $1/T$  for  $B = 5 \text{ T}$  and  $9 \text{ T}$  fitted using the Arrhenius equation (dashed line). (f) Plot of  $(R_0)$  vs.  $(1-h)^{-1/2}$  fitted using the KT equation (dashed line). The inset displays the linear fitted plot of  $(d \ln R_0 / dB)^{-2/3}$  vs.  $B$  to determine the critical  $B$  value ( $B_c = 11 \text{ T}$ ) for the KT transition. The ordered phase at high  $B$  whose origin is intervalley coherent state Kekulé order is also illustrated in the inset.

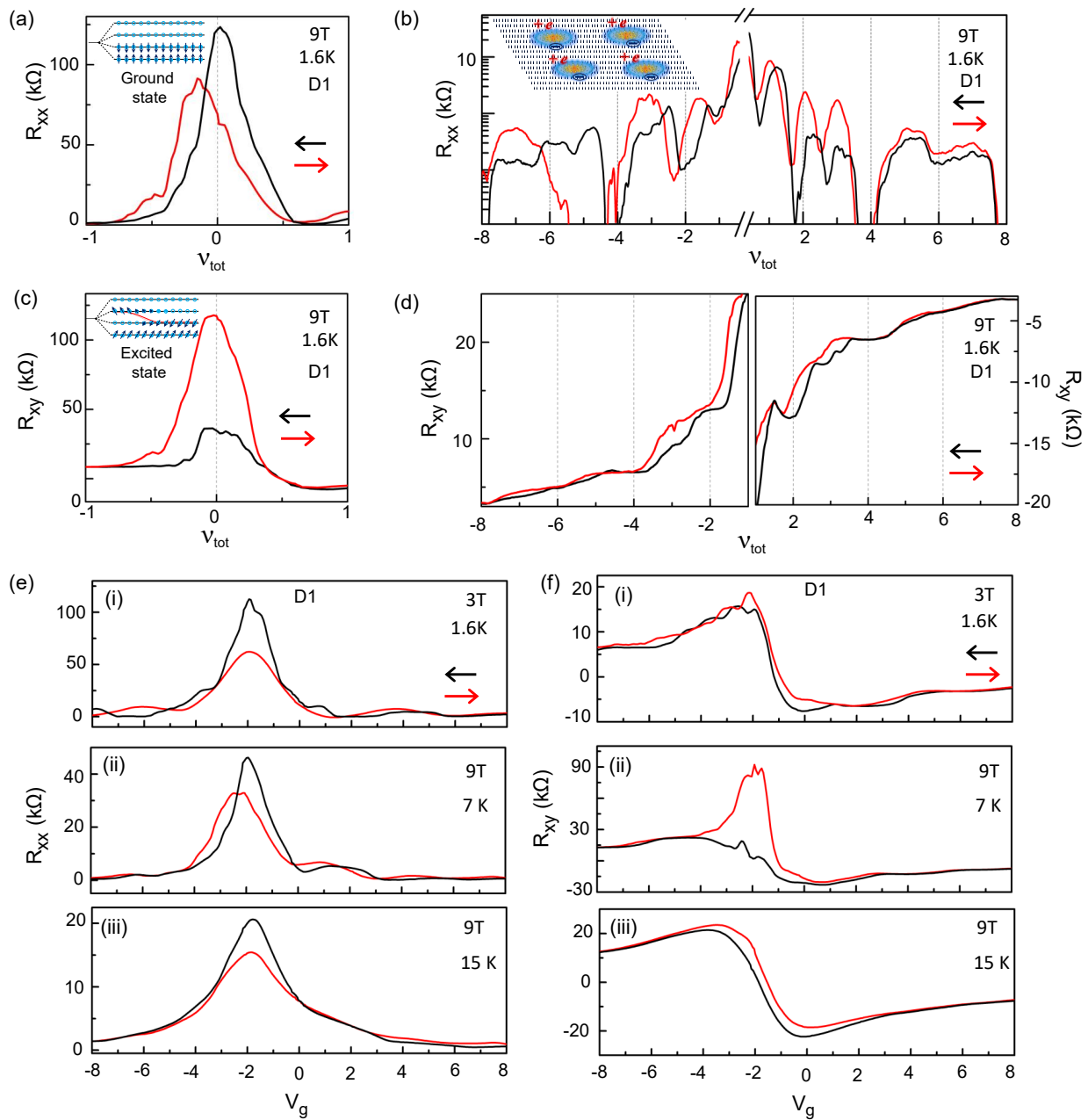


Figure 4: (a) and (b) show dual-sweep measurements of  $R_{xx}$  as a function of  $v_{tot}$  at  $B = 9\text{T}$  and  $T = 1.6\text{K}$ , focusing on  $v_{tot} \approx 0$  and higher  $v_{tot}$  values, respectively. Black and red arrows indicate the direction of the voltage sweep. The inset in (a) shows intervalley coherent state which is the ground state of Kekulé distortion phase, and inset in (c) shows canted antiferromagnetic skyrmion excitation of the Kekulé ordered phase. (c) and (d) show dual-sweep measurements for  $R_{xy}$  as a function of  $v_{tot}$ . Significant hysteresis is observed in both  $R_{xx}$  and  $R_{xy}$ . Inset in (b) shows  $-e$  charge pinned to  $+e$  charged skyrmions. (e) and (f)  $R_{xx}$  and  $R_{xy}$  dual sweeps as a function of  $V_g$  for the conditions : (i)  $B = 3\text{T}, T = 1.6\text{K}$ , (ii)  $B = 9\text{T}, T = 7\text{K}$  and (iii)  $B = 9\text{T}, T = 15\text{K}$ .

## Experimental Methods and Characterisation

**Raman Measurements:** Raman scattering was performed using a WITec alpha300 system equipped with a 532 nm diode laser ( $\sim 16.87$  mW, 500 nm spot size), 1800 lines/mm grating, and a 100 $\times$  objective lens (0.95 NA). Data analysis was carried out using WITec Project software.

**Device Fabrication:** Single-layer graphene (SLG) and hexagonal boron nitride (h-BN) were obtained via mechanical exfoliation of bulk crystals. The h-BN layer was picked up using a PPC/PDMS stamp. TBLG samples were fabricated using the dry transfer method (Cryonano Labs) by sequentially picking up and transferring the top and bottom graphene layers onto pre-exfoliated h-BN on SiO<sub>2</sub>/Si substrate. Devices with edge-contacted Hall bar geometry were patterned using e-beam lithography, followed by CF<sub>4</sub> and O<sub>2</sub> plasma etching of h-BN and graphene. Gold (Au) electrodes (70 nm) were deposited with a titanium (Ti) adhesion layer (10 nm) under a base pressure of 10<sup>-8</sup> mbar in the thermal evaporation chamber.

**Transport Measurements:** Longitudinal ( $R_{xx}$ ) and transverse ( $R_{xy}$ ) resistance measurements were performed using a standard lock-in amplifier with an excitation frequency of  $f = 17.77$  Hz and a current of  $I = 10$  nA, and gate voltage was varied using Keithley 2450 SMU. These experiments were conducted in a Cryostat system (Cryogenics UK) equipped with a superconducting magnet capable of reaching fields up to 9 T.

## Acknowledgement

V.P., A.M.B. and V.K. acknowledge the funding from the Start-up Research Grant from the Science and Engineering Research Board (SERB), Department of Science and Technology (DST), Government of India, and the STEP facility, IIT Kharagpur. V.P., P.G., S.P. and V.K. also acknowledge the DST-Nanomission programme of the Department of Science and Technology, Government of India (DST/NM/TUE/QM-1/2019). R.P. and A.N.P. acknowledge the Thematic Unit of Excellence on Nanodevice Technology (grant no. SR/NM/NS-09/2011) and the Technical Research Centre (TRC) Instrument facilities of S. N. Bose National Centre for Basic Sciences, es-

published under the TRC project of Department of Science and Technology (DST), Govt. of India. A.N.P. acknowledges DST Nano Mission: DST/NM/TUE/QM-10/2019 . K.W. and T.T. acknowledge support from the JSPS KAKENHI (Grant Numbers 21H05233 and 23H02052) , the CREST (JPMJCR24A5), JST and World Premier International Research Center Initiative (WPI), MEXT, Japan.

## References

- (1) Girvin, S. M. Spin and Isospin: Exotic Order in Quantum Hall Ferromagnets. *Physics Today* **2000**, *53*, 39–45.
- (2) Shayegan, M.; Poortere, E. P. D.; Gunawan, O.; Shkolnikov, Y. P.; Tutuc, E.; Vakili, K. Quantum Hall effect in a Multi-valley Two-dimensional Electron Systems. *International Journal of Modern Physics B* **2007**, *21*, 1388–1397.
- (3) He, S.; Xie, X. C.; Sarma, S. D.; Zhang, F. C. Quantum Hall effect in double-quantum-well systems. *Physical Review B* **1991**, *43*, 9339–9342.
- (4) Sarma, S. D.; Pinczuk, A. Perspectives in Quantum Hall Effects: Novel Quantum Liquids in Low-Dimensional Semiconductor Structures. 1997.
- (5) Poortere, E. P. D.; Tutuc, E.; Papadakis, S. J.; Shayegan, M. Resistance Spikes at Transitions Between Quantum Hall Ferromagnets. *Science* **2000**, *290*, 1546–1549.
- (6) Piazza, V.; Pellegrini, V.; Beltram, F.; Wegscheider, W.; Jungwirth, T.; MacDonald, A. H. First-order phase transitions in a quantum Hall ferromagnet. *Nature* **1999**, *402*, 638–641.
- (7) Barrett, S. E.; Dabbagh, G.; Pfeiffer, L. N.; West, K. W.; Tycko, R. Optically Pumped NMR Evidence for Finite-Size Skyrmions in GaAs Quantum Wells near Landau Level Filling  $\nu = 1$ . *Physical Review Letters* **1995**, *74*, 5112–5115.



- (8) Tycko, R.; Barrett, S. E.; Dabbagh, G.; Pfeiffer, L. N.; West, K. W. Electronic States in Gallium Arsenide Quantum Wells Probed by Optically Pumped NMR. *Science* **1995**, *268*, 1460–1463.
- (9) Bayot, V.; Grivei, E.; Melinte, S.; Santos, M. B.; Shayegan, M. Giant Low Temperature Heat Capacity of GaAs Quantum Wells near Landau Level Filling  $\nu = 1$ . *Physical Review Letters* **1996**, *76*, 4584–4587.
- (10) Lay, T. S.; Suen, Y. W.; Manoharan, H. C.; Ying, X.; Santos, M. B.; Shayegan, M. Anomalous temperature dependence of the correlated  $\nu = 1$  quantum Hall effect in bilayer electron systems. *Physical Review B* **1994**, *50*, 17725–17728.
- (11) Murphy, S. Q.; Eisenstein, J. P.; Boebinger, G. S.; Pfeiffer, L. N.; West, K. W. Many-body integer quantum Hall effect: Evidence for new phase transitions. *Physical Review Letters* **1994**, *72*, 728–731.
- (12) Young, A. F.; Dean, C. R.; Wang, L.; Ren, H.; Cadden-Zimansky, P.; Watanabe, K.; Taniguchi, T.; Hone, J.; Shepard, K. L.; Kim, P. Spin and valley quantum Hall ferromagnetism in graphene. *Nature Physics* **2012**, *8*, 550–556.
- (13) Zhao, Y.; Cadden-Zimansky, P.; Jiang, Z.; Kim, P. Symmetry Breaking in the Zero-Energy Landau Level in Bilayer Graphene. *Physical Review Letters* **2010**, *104*, 066801.
- (14) Jiang, Z.; Zhang, Y.; Stormer, H. L.; Kim, P. Quantum Hall States near the Charge-Neutral Dirac Point in Graphene. *Physical Review Letters* **2007**, *99*, 106802.
- (15) Zhang, Y.; Jiang, Z.; Small, J. P.; Purewal, M. S.; Tan, Y.-W.; Fazlollahi, M.; Chudow, J. D.; Jaszczak, J. A.; Stormer, H. L.; Kim, P. Landau-Level Splitting in Graphene in High Magnetic Fields. *Physical Review Letters* **2006**, *96*, 136806.
- (16) Weitz, R. T.; Allen, M. T.; Feldman, B. E.; Martin, J.; Yacoby, A. Broken-Symmetry States in Doubly Gated Suspended Bilayer Graphene. *Science* **2010**, *330*, 812–816.

- (17) Feldman, B. E.; Martin, J.; Yacoby, A. Broken-symmetry states and divergent resistance in suspended bilayer graphene. *Nature Physics* **2009**, *5*, 889–893.
- (18) Datta, B.; Dey, S.; Samanta, A.; Agarwal, H.; Borah, A.; Watanabe, K.; Taniguchi, T.; Sen-sarma, R.; Deshmukh, M. M. Strong electronic interaction and multiple quantum Hall ferro-magnetic phases in trilayer graphene. *Nature Communications* **2017**, *8*, 14518.
- (19) Lee, Y.; Velasco, J.; Tran, D.; Zhang, F.; Bao, W.; Jing, L.; Myhro, K.; Smirnov, D.; Lau, C. N. Broken Symmetry Quantum Hall States in Dual-Gated ABA Trilayer Graphene. *Nano Letters* **2013**, *13*, 1627–1631.
- (20) Liu, K.; Zheng, J.; Sha, Y.; Lyu, B.; Li, F.; Park, Y.; Ren, Y.; Watanabe, K.; Taniguchi, T.; Jia, J.; Luo, W.; Shi, Z.; Jung, J.; Chen, G. Spontaneous broken-symmetry insulator and metals in tetralayer rhombohedral graphene. *Nature Nanotechnology* **2024**, *19*, 188–195.
- (21) Han, T.; Lu, Z.; Scuri, G.; Sung, J.; Wang, J.; Han, T.; Watanabe, K.; Taniguchi, T.; Park, H.; Ju, L. Correlated insulator and Chern insulators in pentalayer rhombohedral-stacked graphene. *Nature Nanotechnology* **2024**, *19*, 181–187.
- (22) Novoselov, K. S.; Geim, A. K.; Morozov, S. V.; Jiang, D.; Katsnelson, M. I.; Grigorieva, I. V.; Dubonos, S. V.; Firsov, A. A. Two-dimensional gas of massless Dirac fermions in graphene. *Nature* **2005**, *438*, 197–200.
- (23) Zhang, Y.; Tan, Y.-W.; Stormer, H. L.; Kim, P. Experimental observation of the quantum Hall effect and Berry’s phase in graphene. *Nature* **2005**, *438*, 201–204.
- (24) Nomura, K.; MacDonald, A. H. Quantum Hall Ferromagnetism in Graphene. *Physical Re-view Letters* **2006**, *96*, 256602.
- (25) Yang, K.; Sarma, S. D.; MacDonald, A. H. Collective modes and skyrmion excitations in graphene  $SU(4)$  quantum Hall ferromagnets. *Physical Review B* **2006**, *74*, 075423.

- (26) Eisenstein, J. P.; Boebinger, G. S.; Pfeiffer, L. N.; West, K. W.; He, S. New fractional quantum Hall state in double-layer two-dimensional electron systems. *Physical Review Letters* **1992**, *68*, 1383–1386.
- (27) Boebinger, G. S.; Jiang, H. W.; Pfeiffer, L. N.; West, K. W. Magnetic-field-driven destruction of quantum Hall states in a double quantum well. *Physical Review Letters* **1990**, *64*, 1793–1796.
- (28) Wiersma, R. D.; Lok, J. G. S.; Kraus, S.; Dietsche, W.; von Klitzing, K.; Schuh, D.; Bichler, M.; Tranitz, H.-P.; Wegscheider, W. Activated Transport in the Separate Layers that Form the  $\nu_T = 1$  Exciton Condensate. *Physical Review Letters* **2004**, *93*, 266805.
- (29) Kellogg, M.; Eisenstein, J. P.; Pfeiffer, L. N.; West, K. W. Vanishing Hall Resistance at High Magnetic Field in a Double-Layer Two-Dimensional Electron System. *Physical Review Letters* **2004**, *93*, 036801.
- (30) Tutuc, E.; Shayegan, M.; Huse, D. A. Counterflow Measurements in Strongly Correlated GaAs Hole Bilayers: Evidence for Electron-Hole Pairing. *Physical Review Letters* **2004**, *93*, 036802.
- (31) Eisenstein, J. P.; MacDonald, A. H. Bose–Einstein condensation of excitons in bilayer electron systems. *Nature* **2004**, *432*, 691–694.
- (32) Cao, Y.; Fatemi, V.; Fang, S.; Watanabe, K.; Taniguchi, T.; Kaxiras, E.; Jarillo-Herrero, P. Unconventional superconductivity in magic-angle graphene superlattices. *Nature* **2018**, *556*, 43–50.
- (33) Cao, Y.; Fatemi, V.; Demir, A.; Fang, S.; Tomarken, S. L.; Luo, J. Y.; Sanchez-Yamagishi, J. D.; Watanabe, K.; Taniguchi, T.; Kaxiras, E.; Ashoori, R. C.; Jarillo-Herrero, P. Correlated insulator behaviour at half-filling in magic-angle graphene superlattices. *Nature* **2018**, *556*, 80–84.

- (34) Bistritzer, R.; MacDonald, A. H. Moiré bands in twisted double-layer graphene. *Proceedings of the National Academy of Sciences* **2011**, *108*, 12233–12237.
- (35) Pezzini, S.; Mišeikis, V.; Piccinini, G.; Forti, S.; Pace, S.; Engelke, R.; Rossella, F.; Watanabe, K.; Taniguchi, T.; Kim, P.; Coletti, C. 30°-Twisted Bilayer Graphene Quasicrystals from Chemical Vapor Deposition. *Nano Letters* **2020**, *20*, 3313–3319.
- (36) Kim, Y.; Moon, P.; Watanabe, K.; Taniguchi, T.; Smet, J. H. Odd Integer Quantum Hall States with Interlayer Coherence in Twisted Bilayer Graphene. *Nano Letters* **2021**, *21*, 4249–4254.
- (37) Wang, L.; Meric, I.; Huang, P. Y.; Gao, Q.; Gao, Y.; Tran, H.; Taniguchi, T.; Watanabe, K.; Campos, L. M.; Muller, D. A.; Guo, J.; Kim, P.; Hone, J.; Shepard, K. L.; Dean, C. R. One-Dimensional Electrical Contact to a Two-Dimensional Material. *Science* **2013**, *342*, 614–617.
- (38) Pandey, V.; Mishra, S.; Maity, N.; Paul, S.; B, A. M.; Roy, A. K.; Glavin, N. R.; Watanabe, K.; Taniguchi, T.; Singh, A. K.; Kochat, V. Probing Interlayer Interactions and Commensurate–Incommensurate Transition in Twisted Bilayer Graphene through Raman Spectroscopy. *ACS Nano* **2024**, *18*, 4756–4764.
- (39) Carozo, V.; Almeida, C. M.; Ferreira, E. H. M.; Cançado, L. G.; Achete, C. A.; Jorio, A. Raman Signature of Graphene Superlattices. *Nano Letters* **2011**, *11*, 4527–4534.
- (40) Fallahazad, B.; Hao, Y.; Lee, K.; Kim, S.; Ruoff, R. S.; Tutuc, E. Quantum Hall effect in Bernal stacked and twisted bilayer graphene grown on Cu by chemical vapor deposition. *Physical Review B* **2012**, *85*, 201408.
- (41) Sanchez-Yamagishi, J. D.; Taychatanapat, T.; Watanabe, K.; Taniguchi, T.; Yacoby, A.; Jarillo-Herrero, P. Quantum Hall Effect, Screening, and Layer-Polarized Insulating States in Twisted Bilayer Graphene. *Physical Review Letters* **2012**, *108*, 076601.
- (42) Schmidt, H.; Lüdtke, T.; Barthold, P.; McCann, E.; Fal’ko, V. I.; Haug, R. J. Tunable graphene system with two decoupled monolayers. *Applied Physics Letters* **2008**, *93*.

- (43) Kim, Y.; Park, J.; Song, I.; Ok, J. M.; Jo, Y.; Watanabe, K.; Taniguchi, T.; Choi, H. C.; Lee, D. S.; Jung, S.; Kim, J. S. Broken-Symmetry Quantum Hall States in Twisted Bilayer Graphene. *Scientific Reports* **2016**, *6*, 38068.
- (44) Liu, X.; Farahi, G.; Chiu, C.-L.; Papic, Z.; Watanabe, K.; Taniguchi, T.; Zaletel, M. P.; Yazdani, A. Visualizing broken symmetry and topological defects in a quantum Hall ferromagnet. *Science* **2022**, *375*, 321–326.
- (45) Coissard, A.; Wander, D.; Vignaud, H.; Grushin, A. G.; Repellin, C.; Watanabe, K.; Taniguchi, T.; Gay, F.; Winkelmann, C. B.; Courtois, H.; Sellier, H.; Sacépé, B. Imaging tunable quantum Hall broken-symmetry orders in graphene. *Nature* **2022**, *605*, 51–56.
- (46) Kharitonov, M. Phase diagram for the  $\nu = 0$  quantum Hall state in monolayer graphene. *Physical Review B* **2012**, *85*, 155439.
- (47) Das, A.; Kaul, R. K.; Murthy, G. Coexistence of Canted Antiferromagnetism and Bond Order in  $\nu = 0$  Graphene. *Physical Review Letters* **2022**, *128*, 106803.
- (48) Delagrangé, R.; Garg, M.; Breton, G. L.; Zhang, A.; Dong, Q.; Jin, Y.; Watanabe, K.; Taniguchi, T.; Roulleau, P.; Maillet, O.; Roche, P.; Parmentier, F. D. Vanishing bulk heat flow in the  $\nu = 0$  quantum Hall ferromagnet in monolayer graphene. *Nature Physics* **2024**, *20*, 1927–1932.
- (49) Nomura, K.; Ryu, S.; Lee, D.-H. Field-Induced Kosterlitz-Thouless Transition in the  $N = 0$  Landau Level of Graphene. *Physical Review Letters* **2009**, *103*, 216801.
- (50) Checkelsky, J. G.; Li, L.; Ong, N. P. Zero-Energy State in Graphene in a High Magnetic Field. *Physical Review Letters* **2008**, *100*, 206801.
- (51) Kosterlitz, J. M. The critical properties of the two-dimensional xy model. *Journal of Physics C: Solid State Physics* **1974**, *7*, 1046–1060.

- (52) Atteia, J.; Lian, Y.; Goerbig, M. O. Skyrmion zoo in graphene at charge neutrality in a strong magnetic field. *Physical Review B* **2021**, *103*, 035403.
- (53) Pierce, A. T.; Xie, Y.; Lee, S. H.; Forrester, P. R.; Wei, D. S.; Watanabe, K.; Taniguchi, T.; Halperin, B. I.; Yacoby, A. Thermodynamics of free and bound magnons in graphene. *Nature Physics* **2022**, *18*, 37–41.
- (54) Lian, Y.; Rosch, A.; Goerbig, M.  $SU(4)$  Skyrmions in the  $\nu = \pm 1$  Quantum Hall State of Graphene. *Physical Review Letters* **2016**, *117*, 056806.

## Supporting Information

### Broken symmetry states and Quantum Hall Ferromagnetism in decoupled twisted bilayer graphene

Vineet Pandey,<sup>†</sup> Prasenjit Ghosh,<sup>†</sup> Riju Pal,<sup>‡</sup> Sourav Paul,<sup>†</sup> Abhijith M B,<sup>†</sup> Kenji Watanabe,<sup>§</sup> Takashi Taniguchi,<sup>||</sup> Atindra Nath Pal,<sup>‡</sup> and Vidya Kochat,<sup>\*,†</sup>

<sup>†</sup>*Materials Science Centre, Indian Institute of Technology, Kharagpur, West Bengal – 721302, India*

<sup>‡</sup>*S. N. Bose National Centre for Basic Sciences, Kolkata, West Bengal- 700106, India.*

<sup>§</sup>*Research Center for Electronic and Optical Materials, National Institute for Materials Science, 1-1 Namiki, Tsukuba 305-0044, Japan*

<sup>||</sup>*Research Center for Materials Nanoarchitectonics, National Institute for Materials Science, 1-1 Namiki, Tsukuba 305-0044, Japan*

\*E-mail: [vidya@matsc.iitkgp.ac.in](mailto:vidya@matsc.iitkgp.ac.in)

#### S1. Raman Spectroscopy of twisted bilayer graphene:

To characterize the twist angle ( $\theta$ ) of our devices, we employed Raman spectroscopy, a widely recognized technique for analyzing twisted bilayer graphene (TBLG). Previous Raman studies [1,2] have established that the R and R' modes, associated with LO phonons, exhibit a strong dependence on the twist angle.

Figure S1(a) presents the optical images of devices D1 and D2. The corresponding Raman maps highlight the overlap regions (dashed outlines) where two monolayer graphene layers form the TBLG system, as shown in Figure S1(b). The Raman spectra for devices D1 and D2 are displayed in Figure S1(c). For device D1, we observed the R' mode around  $1625\text{ cm}^{-1}$ , which corresponds to a twist angle of approximately  $5^\circ$ , consistent with prior Raman studies on TBLG. Similarly, for device D2, the R mode was detected around  $1426\text{ cm}^{-1}$ , indicating a twist angle of approximately  $18^\circ$ .

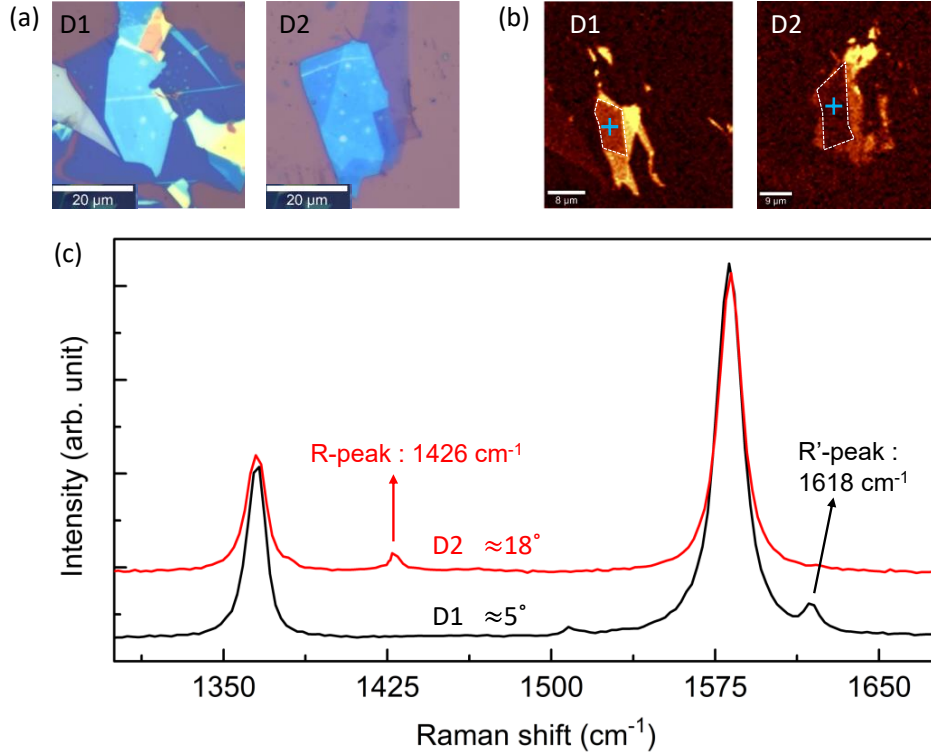


**Figure S1:** (a) Optical images of device D1 and D2. (b) Raman map of TBLG device samples. (c) Raman spectra of devices of D1 and D2.

**S2. Calculation of filling factors of upper ( $\nu_U$ ) and lower ( $\nu_L$ ) layers:**

To investigate how the upper ( $n_U$ ) and lower ( $n_L$ ) layer densities vary with  $V_g$  in TBLG samples, we employ a model designed to calculate the layer densities in graphene double layers that are independently contacted and separated by a dielectric medium [3,4]. The applied back-gate voltage ( $V_g$ ) is distributed between the SiO<sub>2</sub> dielectric and the Fermi energy of the lower graphene layer, described as:

$$e(V_g - V_D) = \frac{e^2(n_U + n_L)}{C_{BG}} + E_F(n_L) \dots \dots \dots (1)$$

where,  $V_D$  is the Dirac point offset and  $C_{BG}$  is the back-gate capacitance of SiO<sub>2</sub> and h-BN. The Fermi energy relative to the charge neutrality point in monolayer graphene at a carrier density  $n$  is given by  $E_F(n) = \text{sgn}(n) \hbar v_f \sqrt{\pi |n|}$ , where  $\text{sgn}(n)$  is signum function and determines the sign of  $n$ , and the Fermi velocity is given as  $v_f \approx 10^8$  cm/s. The  $E_F$  of the lower layer can be expressed as the sum of the electrostatic potential difference between the layers and the Fermi energy of the upper layer:



$$E_F(n_L) = \frac{e^2 n_U}{C_{int}} + E_F(n_U) \dots \dots \dots (2)$$

where  $C_{int}$  is the interlayer capacitance between two layers of TBLG. For device D1, experimental  $n_{U,L}$  vs.  $V_g$  calculated using FFT analysis of SdH data (Figure 2(c)) in main text is linearly fitted with the equation (2), gives interlayer capacitance of  $C_{int} = (5.7 \pm 1) \mu\text{F}/\text{cm}$  as a fitting parameter, which agrees with the theoretically expected interlayer capacitance of Bernal-stacked bilayer graphene [5,6]. By using Eqs. (1) and (2) and using  $C_{int} = 5.7 \mu\text{F}/\text{cm}$ , we calculated  $n_U$  and  $n_L$  and the corresponding  $n_{tot} (= n_U + n_L)$ . The plot for  $n_{U,L}$  vs  $n_{tot}$  shown in Figure S2(a). The Fermi energy depends on both carrier density and magnetic field and is given by  $E_F = E_N$ , where  $E_N = \text{sgn}(N)v_f\sqrt{2e\hbar B|N|}$  is the energy of the  $N^{\text{th}}$  Landau level (LL) in TBLG. Here,  $N = \text{Int}\left[\frac{nh}{4eB}\right]$  represents the LL index, with  $\text{Int}$  denoting the nearest integer function. Using  $n_U$  and  $n_L$  densities we calculated layer filling factors  $\nu_{U,L} = \frac{n_{U,L}\hbar}{eB}$ . The plot  $\nu_{U,L}$  vs  $n_{tot}$  for 3T, 6T and 9T as shown in Figure S2(b). The black and red curve shown as  $\nu_U$  and  $\nu_L$  respectively in Figure 2(f) in the main text extracted from the calculated  $\nu_{U,L}$  corresponding to B in steps of 0.5T and plotted as a function of  $\nu_{tot}$ .

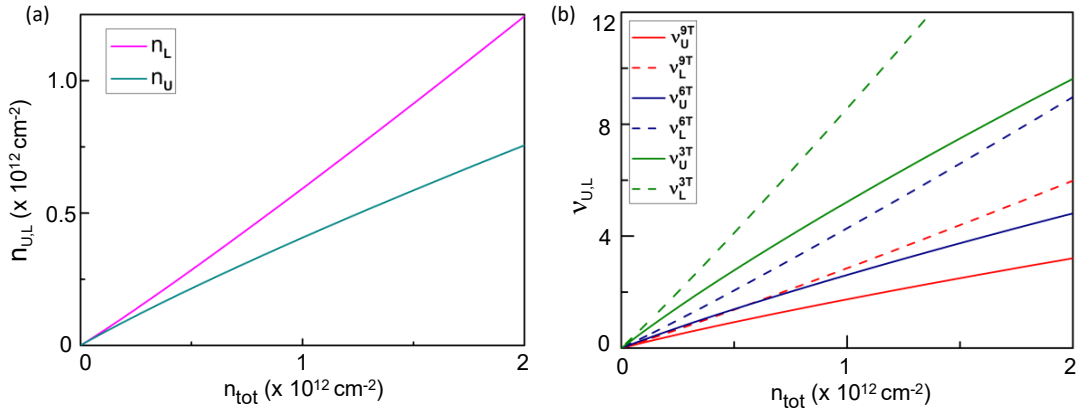


**Figure S2:** (a) Plot for calculated  $n_{U,L}$  vs  $n_{tot}$  for D1. (b) Plot calculated  $\nu_{U,L}$  vs  $n_{tot}$  at 3T, 6T and 9T for device D1.

**S3: Characterization of Device D2 to investigate Quantum Hall (QH) States and magnetoresistance: -**

Device D2 was characterized to explore the emergence of QH states and its magnetoresistance. Figure S3(a) illustrates the longitudinal resistance ( $R_{xx}$ ) as a function of total carrier density ( $n_{tot}$ ) at 300 K and 1.6 K in the absence of a magnetic field. The device exhibited low mobility ( $\approx 18,000 \text{ cm}^2 \text{ V}^{-1} \text{ s}^{-1}$ ) Figure S3(b) presents  $R_{xx}$  versus the total filling factor ( $\nu_{tot}$ ) at 1.6 K under varying magnetic fields (B). Similar to Device D1,  $R_{xx}$  increases at  $\nu_{tot} = 0$  as B increases, but we do not observe a divergent behaviour till 9T. The broken symmetry QH states were also not observed in device D2 till 9T, due to lower mobility. Despite this low mobility and high disorder, QH states were observed at filling factors  $\nu_{tot} = \pm 4, \pm 8, \pm 12, \pm 16 \dots$  similar to D1 (see main text), as shown in Figure S3(b).

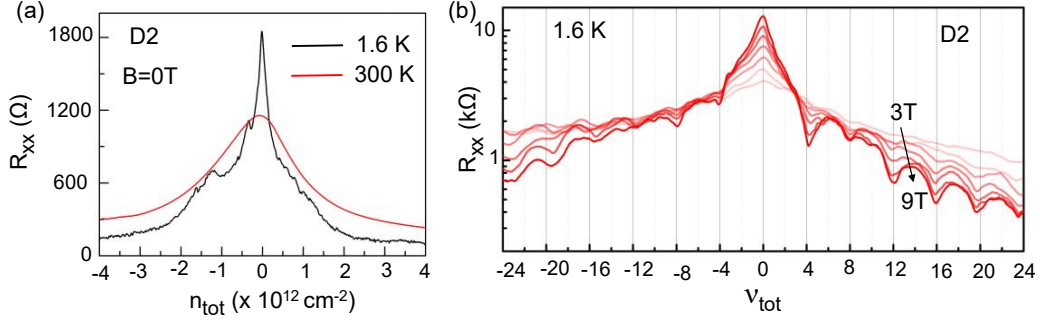


**Figure S3:** (a) Plot for  $R_{xx}$  vs.  $n_{tot}$  at 1.6 K and 300 K at 0T. (b) Plot for  $R_{xx}$  vs.  $\nu_{tot}$  shows QH states.

**S4: Temperature dependence of QH states and SdH oscillations for D1 and D2: -**

Figure S4(a)-(b) depicts the longitudinal resistance ( $R_{xx}$ ) as a function of  $\nu_{tot}$  at different temperatures for Device D1 and D2 respectively. At  $\nu_{tot} = 0$ , highly insulating behavior is observed at low temperatures. As the temperature increases,  $R_{xx}$  at  $\nu_{tot} = 0$  decreases due to the reduction of the QH insulator gap. The  $R_{xx}$  minima at other integral filling factors and the SdH oscillations (in Figure S4(c)-(d)) vanish as temperature is increased due to the thermal broadening and carrier scattering effects when  $k_B T \sim \Delta_{LL}$ , where  $\Delta_{LL}$  is the separation between the LLs.

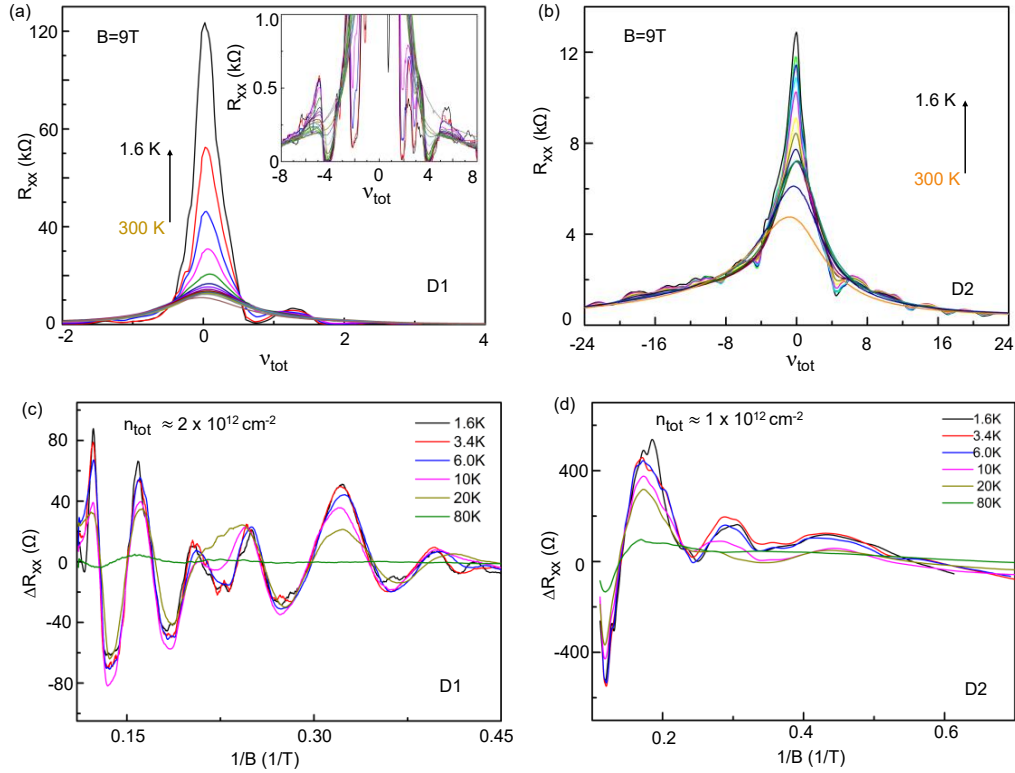


**Figure S4:** (a) Temperature dependence of  $R_{xx}$  vs  $\nu_{tot}$  near the CNP ( $\nu_{tot} = 0$ ) for D1. (inset shows  $R_{xx}$  vs  $\nu_{tot}$  for higher  $\nu_{tot}$  values). (b) Temperature dependence of  $R_{xx}$  vs  $\nu_{tot}$  for D2. (c) and (d) shows temperature dependence of SdH oscillations for D1 and D2 respectively.

### S5: Magnetic field and temperature dependence of Dual sweep $R_{xx}$ for D2: -

Figures S5(a) and S5(b) present the magnetic field (B) and temperature (T) dependence, respectively, of dual sweeps of  $R_{xx}$  as a function of  $v_{tot}$  for Device D2. Unlike Device D1, which exhibits significant hysteresis on both the electron and hole sides (as discussed in the main text), Device D2 shows negligible hysteresis over the range of B and T explored. In the B-dependence data shown in Figure S5(a), the emergence of QH states is observed with increasing magnetic field, consistent with the formation of Landau levels. However, the absence of notable hysteresis, in contrast to Device D1, suggests that hysteresis observed in D1 is most certainly due to the QH ferromagnetism arising from the broken symmetry states.

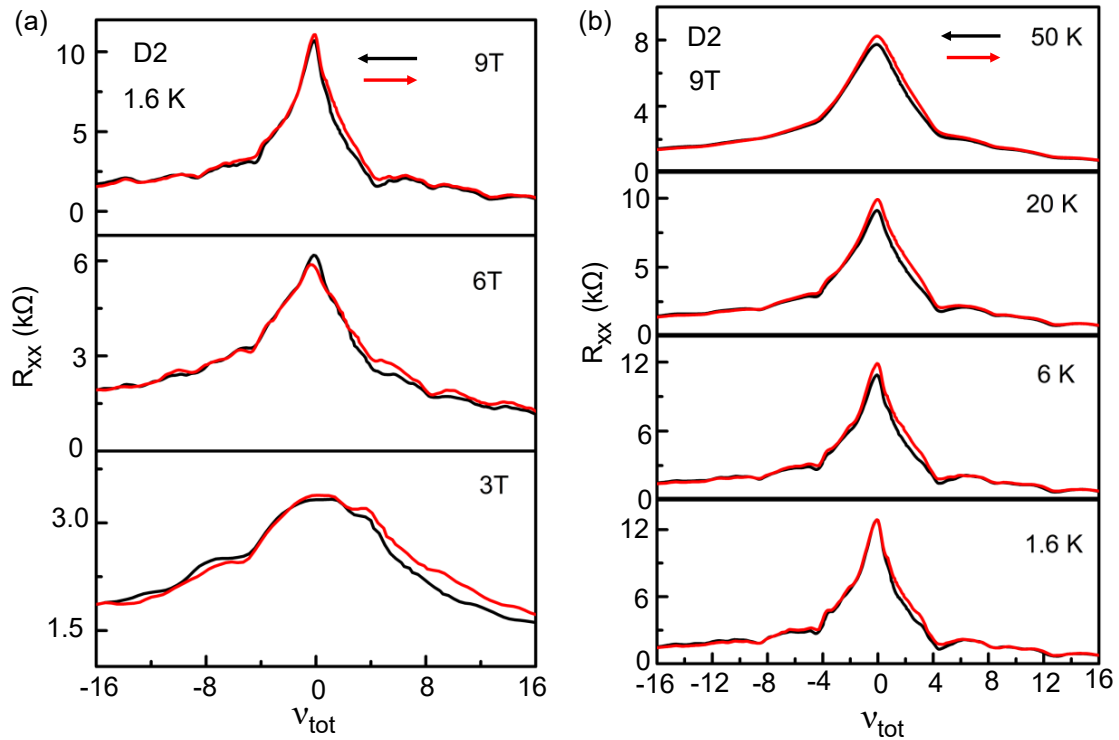


**Figure S5:** (a) Dual sweep  $R_{xx}$  vs  $v_{tot}$  for 3T, 6T and 9T. Black and Red arrow shows the direction of voltage sweep. (b) Temperature dependence of dual sweep  $R_{xx}$  vs.  $v_{tot}$  for 1.6K, 6K, 20K and 50K.

### References

1. Carozo, V.; Almeida, C. M.; Ferreira, E. H. M.; Cancado, L. G.; Achete, C. A.; Jorio, A. Raman Signature of Graphene Superlattices. *Nano Letters* **2011**, 11, 4527–4534.
2. Pandey, V.; Mishra, S.; Maity, N.; Paul, S.; B, A. M.; Roy, A. K.; Glavin, N. R.; Watanabe, K.; Taniguchi, T.; Singh, A. K.; Kochat, V. Probing Interlayer Interactions and Commensurate–Incommensurate Transition in Twisted Bilayer Graphene through Raman Spectroscopy. *ACS Nano* **2024**, 18, 4756–4764.

3. Fallahazad, B.; Hao, Y.; Lee, K.; Kim, S.; Ruoff, R. S.; Tutuc, E. Quantum Hall effect in Bernal stacked and twisted bilayer graphene grown on Cu by chemical vapor deposition. *Physical Review B* **2012**, 85, 201408.
4. Kim, S.; Jo, I.; Nah, J.; Yao, Z.; Banerjee, S. K.; Tutuc, E. Coulomb drag of massless fermions in graphene. *Physical Review B* **2011**, 83, 161401.
5. Min, H.; Sahu, B.; Banerjee, S. K.; MacDonald, A. H. Ab initio theory of gate induced gaps in graphene bilayers. *Physical Review B* **2007**, 75, 155115.
6. Schmidt, H.; Lüdtke, T.; Barthold, P.; McCann, E.; Fal'ko, V. I.; Haug, R. J. Tunable graphene system with two decoupled monolayers. *Applied Physics Letters* **2008**, 93.